Impact of short-term control measures on air quality: A case study during the 7th Military World Games in central China

Yao Mao[a, b, c], Weijie Liu[a, b], Tianpeng Hu[a, b, c], Mingming Shi[a, b], Cheng Cheng[d], Changlin Zhan[e], Li Zhang[e], Jiaquan Zhang[e], Andrew J. Sweetman[c], Kevin C. Jones[c], Xinli Xing[a, b]*, Shihua Qi[a, b]

[a] State Key Laboratory of Biogeology and Environmental Geology, China University of Geosciences, Wuhan 430078, China

[b] School of Environmental Studies, China University of Geosciences, Wuhan 430078, China

[c] Lancaster Environment Centre, Lancaster University, Lancaster, LA1 4YQ, UK

[d] Institute of Hydrobiology, Chinese Academy of Sciences, Wuhan 430072, China

[e] School of Environmental Science and Engineering, Hubei key Laboratory of Mine Environmental Pollution Control and Remediation, Hubei Polytechnic University, Huangshi 435003, China

*Corresponding author: Xinli Xing

Email: xlxing@cug.edu.cn

Abstract:

The 7th Military World Games held in Wuhan (WH) in Oct 2019 provided an opportunity to clarify the impact of short-term control measures on air quality. Filter-based fine particulate matters ($PM_{2.5}$) samples were collected in WH, Huangshi (HS) and Huanggang (HG) during the control (Oct 13-28, 2019) and non-control period (Oct 29- Nov 5, 2019), and its main chemical components were measured, including water-soluble inorganic ions (WSIIs), organic carbon (OC), elemental carbon (EC) and trace elements (TEs). The results showed that air quality was good during the control period, with $PM_{2.5}$ and gaseous pollutants (SO_2, NO_2, CO and O_3) below the China Ambient Air Quality Standard Grade II. Similar $PM_{2.5}$ temporal variations at all sampling sites indicated the regional pollution. Concentrations of $PM_{2.5}$ and its major chemical components were significantly lower in the control period than those in the non-control period, with reductions of 30-45% ($PM_{2.5}$), 22-37% (WSIIs), 18-43% (OC), 23-46% (EC) and 17-52% (TEs), respectively. However, higher contributions of secondary components such as SO_4^{2-}, NO_3^-, NH_4^+ and secondary organic carbon (SOC) to $PM_{2.5}$ were observed

during the control period, suggesting the important role of secondary transformation. Backward trajectory analysis and potential source contribution function (PSCF) showed the main source of $PM_{2.5}$ in WH is local emission, but regional transport can't be ignored, especially for the air masses from HS and HG. Minor variations of As could be affected by air masses from cities to the north with large coal consumption. These results indicated short-term controls were effective for air quality improvement. However, the elevated contribution of secondary components to $PM_{2.5}$ with low primary pollutants and the influence of northern air masses on the study area need more attention for air quality improvement in the future.

Key words: 7th Military World Games; $PM_{2.5}$; Chemical components; Backward trajectory

1 Introduction

Fine particulate matters ($PM_{2.5}$) have adverse effects on human heath, visibility and global climate (Hyslop, 2009; Kim et al., 2015; Pui et al., 2014; Yang et al., 2021). In addition, $PM_{2.5}$ can stay in the atmosphere for a long time and transport long distances, leading to widespread pollution events (Guo et al., 2014). From 2013, air quality across China has been significantly improved, with $PM_{2.5}$ reduction of 30-40% (Li et al., 2019b; Zhang et al., 2019). However, the spatial characteristics of haze pollution has changed. Air quality of typical highly polluted regions, such as Beijing-Tianjin-Hebei region, Yangtze River Delta, Pearl River Delta and Sichuan Basin, is getting better (Li et al., 2020b; Ma et al., 2019; Wu et al., 2021; Yan et al., 2020), while air quality in Twain-Hu Basin which is located in the middle reaches of the Yangtze River is becoming an air pollution hotspot (Li et al., 2020a). Wuhan (WH), the largest megacity in the Twain-Hu Basin, is an important industrial and transportation base, with more than ten million people and three million civil motor vehicles (ending Dec 2018, http://tjj.wuhan.gov.cn/). Studies on the characteristics and causes of air pollution in WH will be of great scientific significance to comprehensively understand the characteristics of the changing atmospheric environment of China.

The 7th Military World Games (MWG) held in WH in Oct 18-27 2019 provided an unprecedented opportunity to understand the chemical characteristics of $PM_{2.5}$ and other air pollutants in real

environment. To ensure the success of the MWG, short-term atmospheric environment quality measures were implemented. There are many successful examples of short-term controls, such as during the Beijing Olympic Games (Schleicher et al., 2012), Shanghai World Expo (Huang et al., 2013), Guangzhou Asian Games (Tao et al., 2015), Beijing APEC (Ansari et al., 2019; Xu et al., 2019), China Victory Day Parade (Wang et al., 2017), and Hangzhou G20 Summit (Chen et al., 2021; Li et al., 2019a). Air quality during these mega-events was improved, with significant $PM_{2.5}$ reduction. However, it is often difficult to fully separate whether emission control or meteorological parameters were responsible for air quality improvement. Some studies reported favorable meteorological conditions were responsible for the good air quality, and emission control had a relatively small impact (Ansari et al., 2019); some suggested primary particulate/gaseous pollutants emission control is the most effective way to reduce $PM_{2.5}$ (Su et al., 2021; Wang et al., 2017). However, pollution episodes can also be observed during the control periods, with other increased sources (e.g. enhanced heating), unfavorable meteorological conditions and regional atmospheric transport (Wang et al., 2017; Zhang et al., 2020). In short, emission control measures (often at huge economic cost) may have some positive influence on $PM_{2.5}$ reduction, but its effectiveness depends on a variety of factors. Thus the trade-off between air quality improvement and the cost emission controls should be considered.

The source and formation mechanism of $PM_{2.5}$ are different in different regions. Unlike urban agglomerations such as Beijing and Shanghai, WH is located in the Jianghan Plain, surrounded by mountains and cities. The effect of control measures on air quality and $PM_{2.5}$ chemical composition variations in WH and surrounding cities is unclear. Therefore, filter-based $PM_{2.5}$ samples, gaseous pollutants and meteorological parameters were collected in WH and surrounding cities (Huangshi City (HS) and Huanggang City (HG)) which lie to the east of WH during this campaign, in order to: (1) assess air quality during the 7th MWG in WH and surrounding cities; (2) explore the effect of emission control and meteorological parameters on $PM_{2.5}$ through its chemical composition variation; and (3) provide reasonable suggestions for further control of particulate pollution in WH and other mega-events. Importantly, the short-term introduction of control measures provided an opportunity to assess the relative contributions of local (city) sources and regional transport for WH and surrounding areas.

2 Methodology

2.1 Control scheme, study area and sample collection

The meteorological conditions in WH in Oct are characterized by low precipitation, low wind speed, high relative humidity and frequent temperature inversion in recent years, which are not conducive to the dispersion of air pollutants. Local emissions contribute a lot to $PM_{2.5}$ in WH, and long-range transport cannot be ignored, due to winds from industrialized and populated regions the north. To ensure air quality during the 7th MWG, atmospheric environment quality management measures were implemented in Hubei Province from Oct 13 to Oct 28 2019, especially in WH (http://www.wuhan.gov.cn/). According to source apportionment estimates (from Wuhan Municipal Ecology and Environment Bureau), $PM_{2.5}$ in WH mainly comes from industry (32%), vehicle emission (27%), coal combustion (20%), dust (9%) and others (such as cooking, biomass burning and agricultural activities, 12%). Therefore, control measures mainly targeted coal-fired power plants and coke ovens, the cement industry, construction work, non-road motor vehicles, ships and airplanes, while there was no strict control for private cars and buses to minimize the impact on people's lives. However, trucks were banned from entering the third ring road of WH. When control measures were implemented, the government expected that air pollutant emissions could be reduced by more than 40% compared to those in 2018. In conclusion, emission control measures introduced at this time mainly focused on coal-fired power plants and industries, construction work and road dust, which are usually related to primary emission and secondary formation of $PM_{2.5}$.

To evaluate the impact of these control measures on air quality, continuous synchronous observations were carried out in WH, HG and HS from Oct 13 to Nov 5 2019. For comparison, the entire observation period was divided into the control period (Oct 13-Oct 28) and non-control period (Oct 29-Nov 5), based on the timing of control measures implemented. Because the WMG venues were distributed in various districts, five sampling sites were selected in WH, including Yangtze University (site 1), Wuhan University of Science and Technology (Qingshan Campus, site 2), Wuhan University of Science and Technology (Huangjiahu Campus, site 3), China University of Geosciences (Nanwangshan Campus, site 4), and China University of Geosciences (Future City Campus, site 5).

Among them, site 2 and 4 are located within the second and third ring road, representing urban sites. Site 3 is situated close to Huangjia Lake, close to the Military Village (a gathering place for athletes, about 2km away), while sites 1 and 5 are located to the west and east of WH, respectively, representing suburban sites. Furthermore, simultaneous sampling was conducted in HG (sampling site: Huanggang Environmental Monitoring Station, site 6) and HS (sampling site: Hubei Polytechnic University, site 7) to understand the influence of surrounding cities to WH air quality during the MWG. HS is an industrial city with coal-fired metal smelting and cement plants, while HG is known for its agriculture. Detailed information of sampling sites are shown in Fig.1 and Table S1. All sampling sites were located on the roof of a residential building or teaching building (10-20 m above the ground), surrounded by residential or commercial buildings, with no large-scale industrial emission sources within 5 km.

Integrated $PM_{2.5}$ (09:00 to next day 09:00) samples were simultaneously collected by medium-volume (100 L min^{-1}) samplers (TH-150F, Wuhan Tianhong Instruments Co. Ltd) with quartz fibre filters (Φ=90 mm, Whatman, UK). Before sampling, quartz fibre filters were baked at 550 ℃ for 4 h in a muffle furnace to remove impurities. Then, filters were conditioned for 48 h at a temperature of 25±1℃ and RH of 50±5%, and weighed by a microbalance (T-114, Sartorius Company, Germany) with precision of 0.01 mg before and after sampling. After sampling and weighing, filters were cut into several pieces for chemical analysis, including water-soluble inorganic ions (WSIIs), organic carbon (OC), elemental carbon (EC), trace elements (TEs), and kept in filter storage boxes at -20 ℃ until analysis.

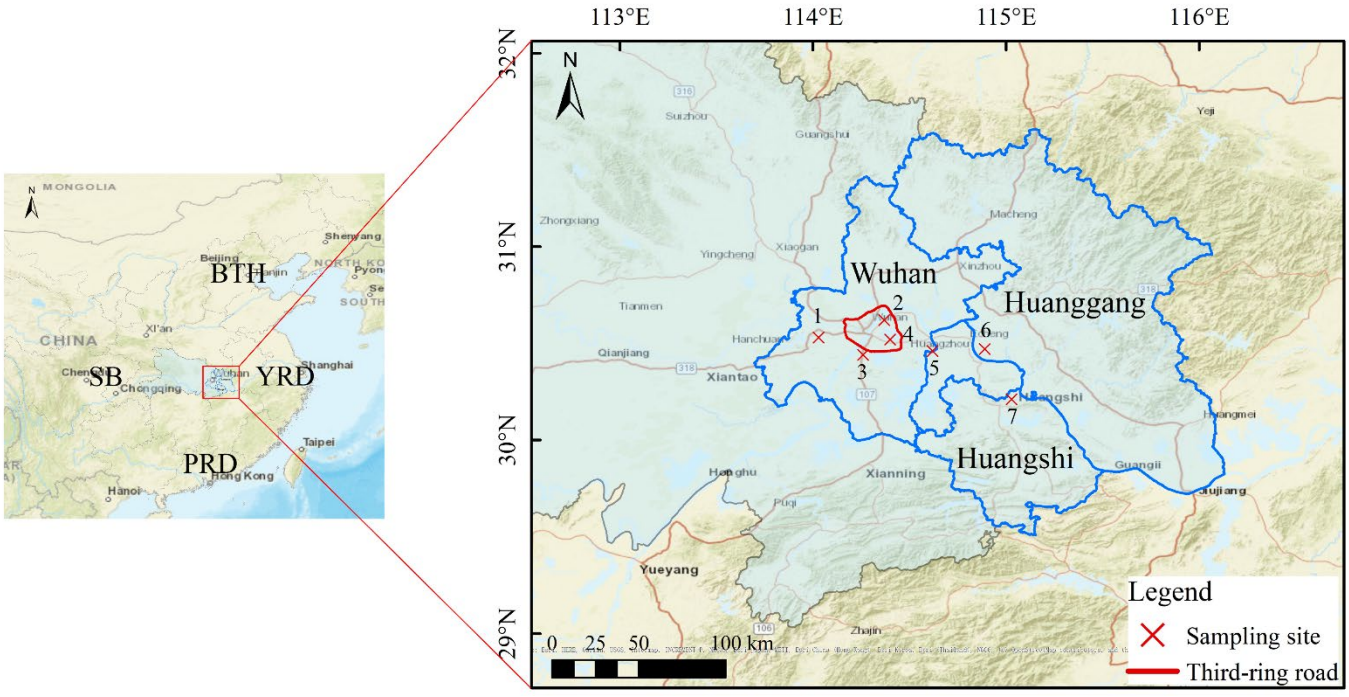

Fig.1 Location of sampling sites (1 Yangtze University, 2 Wuhan University of Science and Technology (Qingshan Campus), 3 Wuhan University of Science and Technology (Huangjiahu Campus), 4 China University of Geosciences (Nanwangshan Campus), 5 China University of Geosciences (Future City Campus), 6 Huanggang Environmental Monitoring Station, 7 Hubei Polytechnic University)

BTH: the Beijing-Tianjin-Hebei region; YRD: Yangtze River Delta; PRD: Pearl River Delta; SB: Sichuan Basin

2.2 Chemical analysis

2.2.1 WSIIs

Two circles of 10 mm diameter were accurately cut from the quartz fibre filters, put into a 15 mL polypropylene tube and then extracted with 10 mL ultrapure water (18.2 MΩ cm) for 45 min in an ultrasonic ice-water bath and shaken for 60 min. The extracts were filtered with a PTFE syringe filter (0.22 μm). Then, about 5 mL solution was taken into a poly vial for instrumental analysis. Five cations (Na^+, NH_4^+, K^+, Mg^{2+}, and Ca^{2+}) and three anions (Cl^-, NO_3^-, and SO_4^{2-}) were determined by ion chromatography (IC, Dionex ICS-1000, USA).

2.2.2 OC and EC

OC and EC concentrations were determined by DRI Model 2015 multiwavelength thermal/optical

carbon analyzer following the IMPROVE_A thermal/optical reflectance (TOR) protocol, which can be found elsewhere (Zhang and Kang, 2018). Briefly, a punch of 0.5026 cm^2 quartz fibre filter was accurately cut and placed on the filter loading. Then, different carbon fractions (OC1, OC2, OC3, OC4, pyrolyzed organic carbon (POC), EC1, EC2, and EC3) were determined by a non-dispersive infrared detector (NDIR) at different oven temperatures (from room temperature to 840℃) and conditions (OC: 100% helium; EC: 98% helium and 2% oxygen). According to IMPROVE_A, OC=OC1+OC2+OC3+OC4+POC, EC=EC1+EC2+EC3-POC (Chow et al., 2007).

2.2.3 Trace elements

A quarter of quartz fiber filter was cut into pieces and placed into a Teflon digestion vessel with an acid mixture of HNO_3 and HF. Each sample was treated with 2 mL HNO_3 at 80℃ for 6 h and 1 mL HF at 180 ℃ for 48 h. The digestion solution after drying was added to 2 mL 30% HNO_3, continuing to digest at 180 ℃ for 12 h, then diluted to 10mL with 1% HNO_3 solution. Ten trace elements (V, Cr, Mn, Co, Ni, Cu, Zn, As, Cd and Pb) were measured by Inductively Coupled Plasma Mass Spectrometry (ICP-MS, PerkinElmer 350D).

2.2.4 QA&QC

All standard solutions of 8 WSIIs and 10 TEs were obtained from o2si US. Laboratory blanks, field blanks, and parallel samples (every 10 samples) were analyzed for target compounds.

For WSIIs analysis, an increasing concentration of calibration standard (0.01, 0.05, 0.1, 0.5, 1, 2, 5, and 10 mg L^{-1}) were used for quantitation and their correlation coefficients were all >0.999. The limit of detection (LOD) for target ions ranged from 0.001 to 0.012 μg m^{-3}. Relative standard deviation (RSD) for parallel samples was <10%.

For carbon analysis, the instrument was calibrated each day with CH_4/CO_2 standard gas before and after sample analysis. LOD was <0.1 μg m^{-3} for OC and EC. RSD for parallel samples was <5%. No OC and EC was detected in blanks.

For trace elements analysis, an increasing concentration of calibration standard (1, 10, 100 μg L^{-1}) was used for quantitation and their correlation coefficients were all >0.9999. LOD for trace elements ranged from 0.001 to 0.005 μg m^{-3}. Relative standard deviation (RSD) for parallel samples was <10%. No target trace element was detected in blanks.

2.3 Complementary data

Hourly data sets of pollutants concentration ($PM_{2.5}$, SO_2, NO_2, CO, O_3) and meteorological parameters (ambient temperature, pressure, relative humidity, wind direction and wind speed) at each sampling site in 2018 and 2019 were obtained from local monitoring stations, which are only a few kilometers from the corresponding sampling sites, so they share similar conditions. Daily data sets of pollutants concentration in WH (2015-2019), HG (2018-2019) and HS (2018-2019) were obtained from the China Air Quality Online Monitoring and Analysis Platform (https://www.aqistudy.cn/). There was significant correlation (p<0.001) between local monitoring station $PM_{2.5}$ concentrations and our filter-based $PM_{2.5}$ concentrations. Therefore, pollutants concentrations (including $PM_{2.5}$, SO_2, NO_2, CO, O_3) from the online platform were selected for the comparison among different years, while SO_2, NO_2, CO, O_3 from local monitoring stations and $PM_{2.5}$ from filter-based sampling were selected for the comparison between control and non-control periods.

2.4 Backward trajectory analysis

48-hour air mass backward trajectories were calculated by the National Oceanic and Atmospheric Administration (NOAA) HYSPLIT model, with meteorological data (1°×1°) obtained from the Global Data Assimilation System (GDAS) for control and non-control periods separately. The model was run for 1-hour intervals each day with starting height of 500 m above ground level. Potential source contribution function (PSCF) has been widely used to explore the potential geographic origins of pollutants (Liu et al., 2018b; Zheng et al., 2019). The PSCF value is the conditional probability that pollutant concentration is greater than a set criterion. More information on PSCF can be found elsewhere (Zheng et al., 2019). The height of the planetary boundary layer (PBL) used in the analysis was obtained from model outputs.

3 Results and discussions

3.1 Overview of air quality in WH and surrounding cities

In general, good air quality in WH, HG and HS was found during the control period (Fig.2), with

daily $PM_{2.5}$ concentration (mean±standard deviation, μg m^{-3}) of 54.2±10, 54.4±11.9 and 60±7.6, respectively, lower than the China Ambient Air Quality Standard Grade II (CAAQS, 75 μg m^{-3} for 24-h average). The lowest $PM_{2.5}$ concentration (35.4 μg m^{-3}) was measured at site 4 in the control period and the highest $PM_{2.5}$ concentration (133.2 μg m^{-3}) was found at site 1 in the non-control period. SO_2, NO_2, CO and O_3 were below the CAAQS Grade II of 150 μg m^{-3}, 80 μg m^{-3}, 4 mg m^{-3} and 160 μg m^{-3}, except for three days at site 2 (Oct 30-31 and Nov 1) with an elevated concentration of NO_2. Similar $PM_{2.5}$ temporal variations at all sampling sites indicated the important role of regional transport.

Compared with the non-control period, $PM_{2.5}$, SO_2, NO_2 and CO were lower in the control period by 38.1-44.8%, 30.9-41.5%, 34.6-39.9% and 0-27.3%, respectively, which could be attributed to the effectiveness of control measures. Compared with the same period (Oct 13-28) in 2018 (Fig. S1), concentrations of $PM_{2.5}$, SO_2, NO_2 and CO in WH decreased by 25%, 15%, 17% and10%, respectively; while, they decreased by 50% ($PM_{2.5}$), 69% (SO_2), 20% (NO_2) and 28% (CO) when compared with the average concentration of the same period in the previous five years (2014-2018). Previous studies showed that the effect on air quality of short-term control measures before 2017 is significantly greater than that after 2017 in China. $PM_{2.5}$ concentration decreased by 45%, 74.6%, and 50% during APEC (2014) (Xu et al., 2019), Military Parade (2015) (Wang et al., 2017) and G20 Summit (2016) (Li et al., 2019a), respectively, when compared with the same period of their previous year; while the reduction of $PM_{2.5}$ concentration was 26% during the BRICS summit in 2017 in Xiamen (Wang et al., 2021). In addition, during the COVID-19 lockdown in WH, when most emission sources were cut, the $PM_{2.5}$ concentration only dropped by 37% (Zheng et al., 2020), which was less than that in mega-events held before 2017. The different downward trend is due to the general success of China's air pollution prevention and control action plan, which started in 2013 (Li et al., 2019b; Zhang et al., 2019), resulting in significant improvement of air quality in WH since 2016 (Huang et al., 2019). It also reflects the effectiveness of control measures implemented during this campaign.

Different from $PM_{2.5}$, the O_3 concentration increased about 22.4% when compared with that in 2018. This was consistent with many previous studies (Li et al., 2019a; Xu et al., 2019; Zheng et al., 2020), suggesting the complexity of air pollution control. Although O_3 was 6.6%-15.4% lower in the control period than in non-control period in general, it presented high concentration during the MWG

period. Many previous studies on short-term control events observed elevated O_3 concentrations due to less NO_x emissions or stronger photochemical reactions during the control period (Xu et al., 2019). Reductions (2018 vs. 2019) of $PM_{2.5}$ and NO_2 observed in HS (14.4% and 15.6%) and HG (18.8% and 1.6%) were not as great as those in WH, indicating air quality assurance measures implemented during this campaign could have more influence on WH than HS and HG. SO_2 concentrations increased, rather than dropping, in HS (26.9%) and HG (18.4%) from 2018 to 2019, indicating variations in pollutants concentrations are influenced by a variety of factors in addition to emission source. Additionally, a higher increase (2018 vs. 2019) of O_3 was found in WH (22.4%) than in HG (6%) and HS (8.9%).

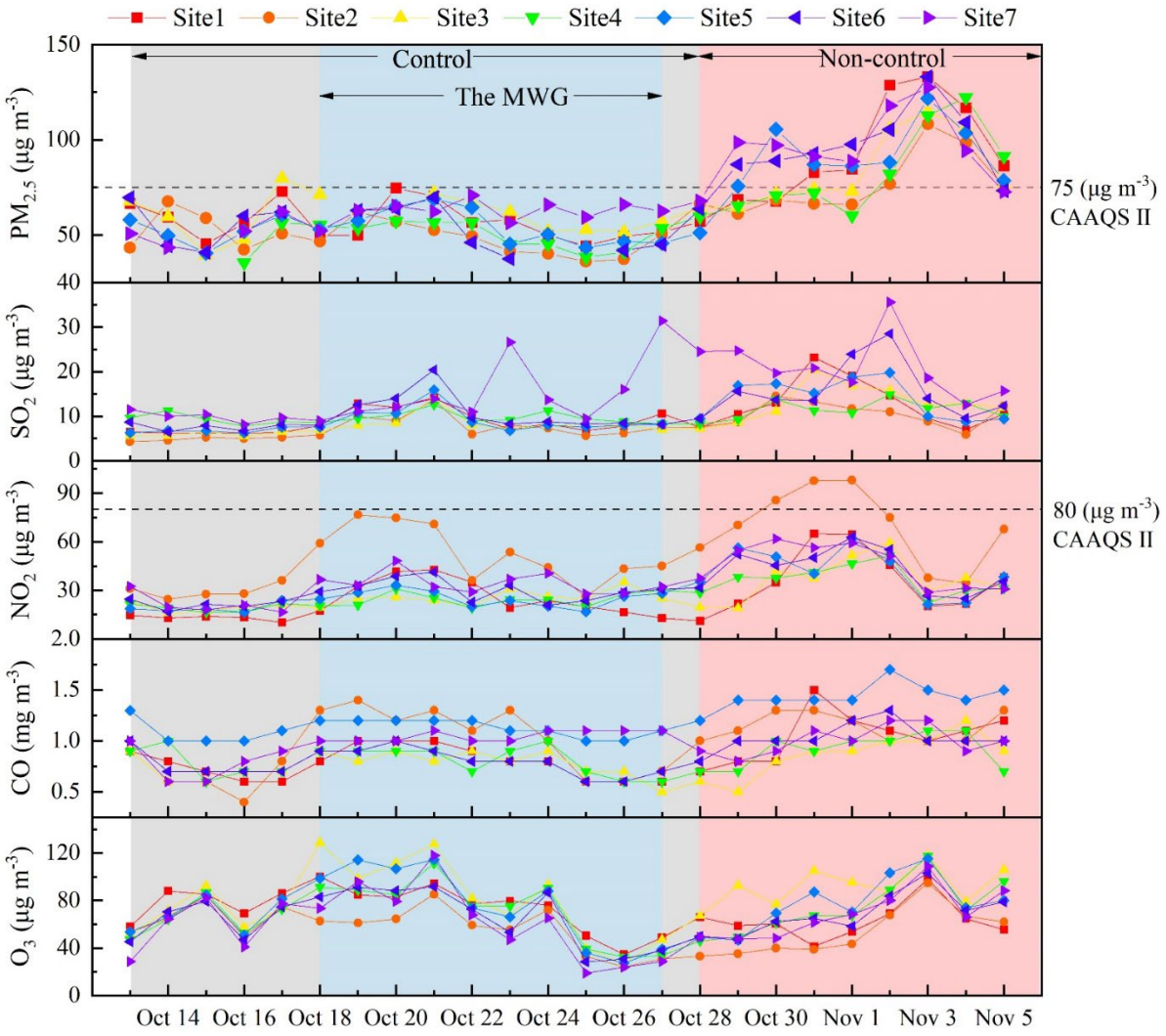

Fig.2 Time series of $PM_{2.5}$ and gaseous pollutants (Grey: control period of Oct 13-28; Blue: the MWG period of Oct 18-27; Red: non-control period of Oct 29-Nov 5)

238

239 **3.2 Air mass transport and meteorological parameters**

240 3.2.1 Meteorological parameters

241 As shown in Table 1, meteorological parameters were similar for the same period in 2018 and
242 2019 in WH, HS and HG, respectively, suggesting atypical meteorological conditions during the
243 control period. Thus, the reduction of pollutants during the control period in this campaign could be
244 mainly caused by the decreasing emission sources. Compared with the meteorological parameters
245 between the control and non-control period (Table 1 and Fig.3), the average wind speed and
246 atmospheric pressure were similar. Northerly winds (Fig.S2) prevailed during the entire observation
247 period at each site, except for HG (prevailing in southeasterly winds). Lower temperatures (18.3 ℃,
248 18.8 ℃ and 18.6 ℃ for WH, HG and HS) with higher relative humidity (74%, 62%, 64%) during the
249 control period were observed than those in the non-control period (19.6 ℃ and 60%, 19.7 ℃ and 51%,
250 19.6 ℃ and 54%). High relative humidity is favorable to the hygroscopic growth of particulate matter
251 and may promote the secondary formation of pollutants, while low temperature could reduce the rate
252 of chemical reaction (Gao et al., 2017).

253 Table 1 Meteorological parameters during control and non-control period in 2019 and the same period in 2018

Meteorological parameters	WH			HG			HS		
	2018	2019 C	2019 N	2018	2019 C	2019 N	2018	2019 C	2019 N
Wind speed (m s^{-1})	1.43	1.09	1.14	0.81	0.89	0.74	4.86	4.51	4.57
Pressure (hPa)	1013.5	1014.3	1013.3	1013.5	1014.6	1013.5	1011.4	1012.4	1011.4
Temperature (℃)	17.6	18.3	19.6	17.8	18.8	19.7	17.5	18.6	19.6
Relative humidity (%)	76	74	60	70	62	51	71	64	54

254 2019 C: Control period in 2019;
255 2019 N: Non-control period in 2019;
256 2018: the same period as 2019 C

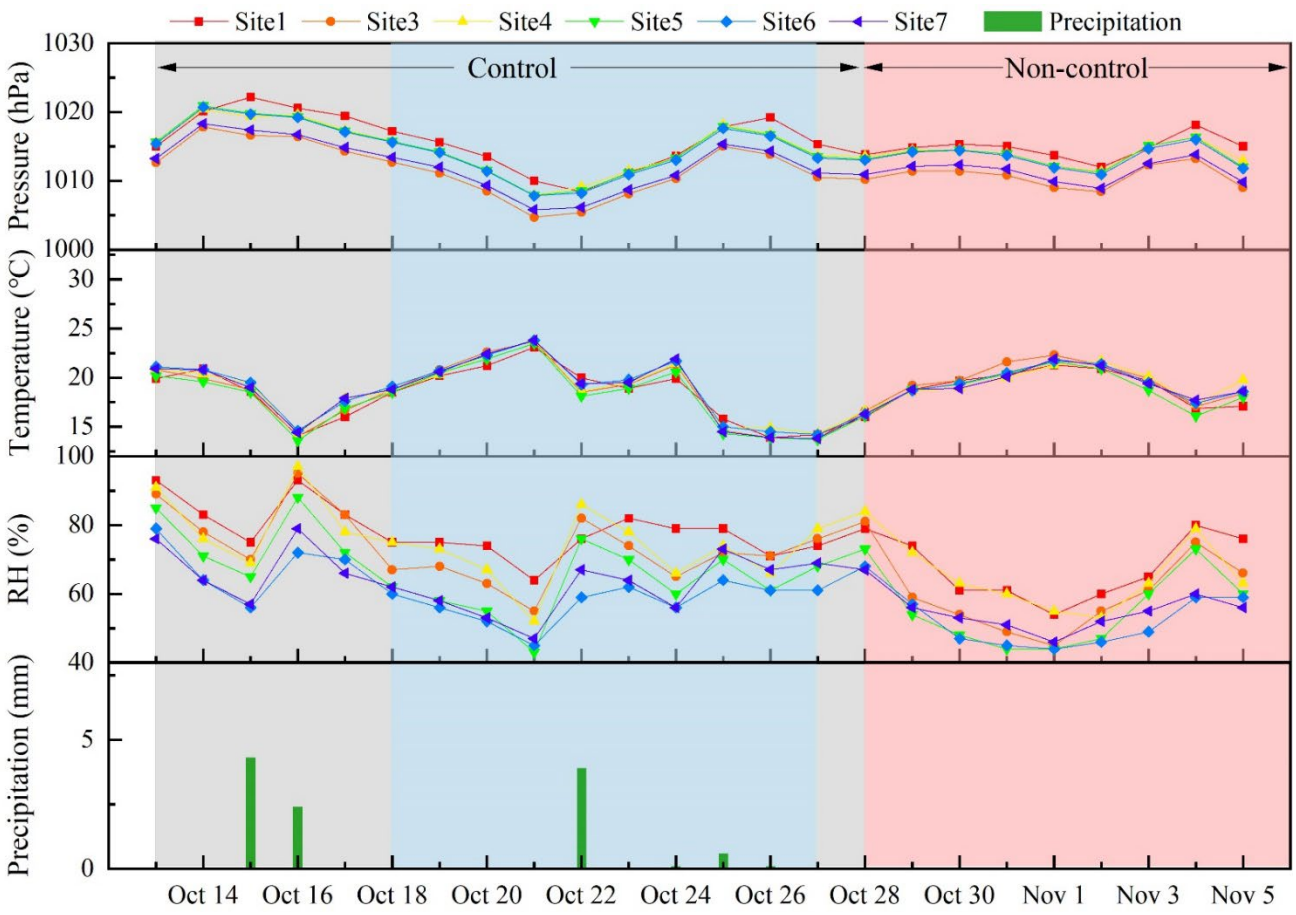

Fig.3 Time series of atmospheric pressure, temperature, relative humidity (RH) and precipitation (Grey: control period of Oct 13-28; Blue: the MWG period of Oct 18-27; Red: non-control period of Oct 29-Nov 5)

As shown in Fig. 2, a low $PM_{2.5}$ concentration was found on Oct 15 (average of 45.0±8.1 μg m^{-3}), which can be attributed to the increasing wind speed and precipitation. Many previous studies have shown that high wind speed and rainfall are effective in removing fine particles (Tao et al., 2017). However, $PM_{2.5}$ began to increase from Oct 16 and peaked on Oct 17 (64.7±10.2 μg m^{-3}), which may be related to the poor dispersion conditions with low wind speed (from 2.3±1.6 m s^{-1} to 1.7±1.1 m s^{-1}) and low PBL (from 573±419 m to 422±454 m), and favorable chemical reaction and hygroscopic growth condition with increasing relative humidity (from 65±8% to 75±8%). Then it maintained a low $PM_{2.5}$ concentration until Oct 28, followed by an increase when control measures finished.

3.2.2 Air mass transport

The results of 48-h backward air mass trajectory and cluster analysis (Fig.S3) showed that air masses reaching at each sampling site were mainly from the northeast (45.31%-84.9% for control period, and 48.96%-55.73% for non-control period), which was related to the prevailing wind direction

during sampling season. In Oct, Hubei Province was during the transition period from summer monsoon to winter monsoon (Huang et al., 2019). Although the air masses were mainly from the northeast, they had different source regions during different periods. For instance, during the control period, air masses reaching at site 3 mainly came from Anhui Province (53.13%), followed by Yellow Sea (18.75%), Inner Mongolia (15.1%) and Hebei Province (13.02%). During the non-control period, site 3 was mainly affected by local and surrounding urban air masses (31.25%), followed by Yellow Sea (28.13%), Zhejiang Province (25.52%) and Shanxi Province (15.1%).

As shown in Fig.S4, high PSCF values mainly occurred in WH, HS, HG, central Anhui Province, and southeastern Henan Province during the control period, but mainly occurred in local regions during the non-control period. As the central city of Wuhan Urban Agglomeration, WH has a large amount of pollutant emissions due to the large population (permanent urban population >9 million in 2019 according to statistical yearbook of WH), car ownership (civil cars >3 million) and rapid industrial development (GDP >1.6 trillion Yuan). Besides, adverse meteorological conditions in Oct and adverse terrain, with its three sides surrounded by mountains, were unfavorable for pollutant dispersion. HS and HG are located on the channel allowing $PM_{2.5}$ movement from the northeast to WH, which has an important influence on air quality in the Wuhan Urban Agglomeration. In addition, HS and HG are often listed among the cities with the worst air quality in Hubei Province, due to high industrialization and dense population. Henan, an inland province, is one of the most populated provinces and the most polluted areas across China (Liu et al., 2018b). Anhui now has become the most heavily polluted area in the YRD, due to its rapid development of industrialization and important role in agricultural production (Mi et al., 2019). To sum up, $PM_{2.5}$ in WH are mainly attributed to local emission. However, regional transport cannot be ignored, especially in the control period.

To explore the effectiveness of local emission reduction, air masses coming from the same area were compared between the control and non-control periods. Two cases were chosen, Oct 21 vs. Oct 31 (case 1) and Oct 22 vs. Nov 4 (case 2), as shown in Fig.3. In case 1, air mass originated from Anhui Province, passing through HG, then reaching site 3. In case 2, air mass originated from the Yellow Sea, passing through Jiangsu Province, Anhui Province, and HG, then reaching site 3. In these two cases, $PM_{2.5}$ concentrations were lower in the control period (72.7 μg m^{-3} and 66.9 μg m^{-3}) than the non-

control period (74.2 μg m^{-3} and 106.3 μg m^{-3}). As similar meteorological parameters were found between control and non-control periods for these two cases (Table 2), the lower $PM_{2.5}$ concentration observed in the control period might not only be related to meteorological parameters, but also to the implementation of emission control measures.

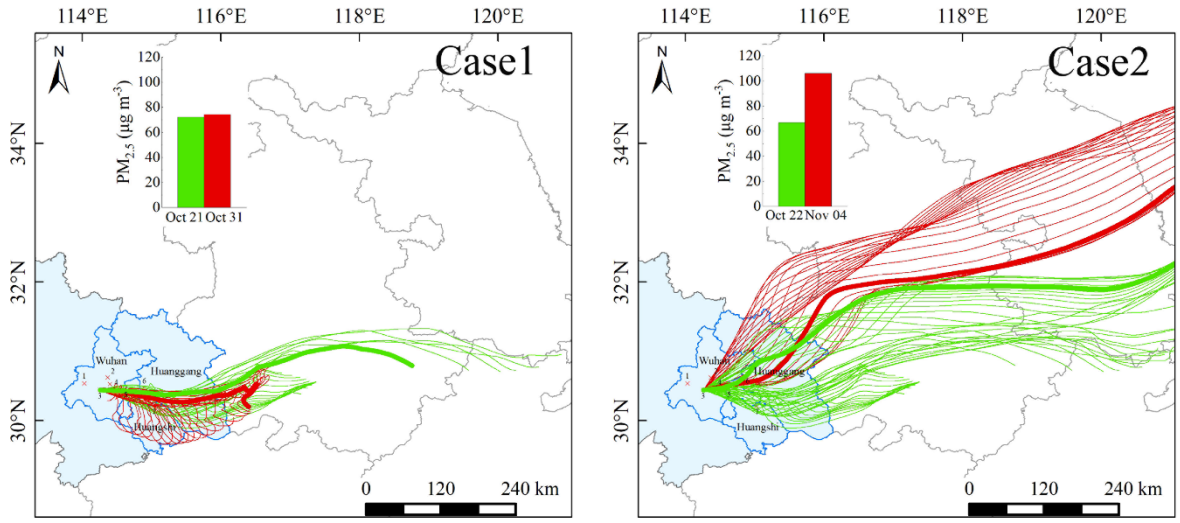

Fig.4 Case study of air mass from the same area during control (green) and non-control period (red)

Case1-Oct 21 vs. Oct 31; Case 2-Oct 22 vs. Nov 04

Table 2 $PM_{2.5}$ concentration and meteorological conditions for two case studies

	Case 1 (Oct 21 vs. Oct 31)		Case 2 (Oct 22 vs. Nov 4)	
	Control	Non-control	Control	Non-control
$PM_{2.5}$ (μg m^{-3})	72.7	74.2	66.9	106.3
WS(m/s)	1.94	2.05	2.28	1.92
RH(%)	55	49	82	75
Temperature(°C)	23.7	21.6	18.5	17.1
Pressure(hPa)	1004.7	1010.8	1005.4	1013.2
PBL(m)	342	220	460	401

3.3 Chemical composition variation

3.3.1 WSIIs

Average concentration of WSIIs in $PM_{2.5}$ were shown in Table 3. In general, concentrations of

WSIIs were 21.6±6.1 μg m^{-3}, 19.7±5.5 μg m^{-3} and 18.3±5.3 μg m^{-3} for WH, HS and HG during the control period, respectively, with significant reductions of 25.0%, 37.5% and 35.6% compared with those in the non-control period. The lower concentration of WSIIs observed in the control period was mainly due to the reduction of SNA (including SO_4^{2-}, NO_3^-, and NH_4^+). SNA were the major components of $PM_{2.5}$, accounting for 25.4-34.0% of $PM_{2.5}$ mass concentration during the entire observation, which fell into the range of previous studies that SNA accounted for 25-48% of $PM_{2.5}$ mass concentration in China (Tao et al., 2017). Reduction (decreased by 18.6-37.2%) of SNA concentration with elevated (increased by 8.8-45.6%) contribution of SNA to $PM_{2.5}$ during the control period indicated the important role of secondary transformation on $PM_{2.5}$ variation.

Table 3 Mass concentration of water-soluble inorganic ions during control and non-control period

Species	WH[a] (n=115)			HG (n=21)			HS (n=23)		
(μg m^{-3})	Mean	Control	Non-control	Mean	Control	Non-control	Mean	Control	Non-control
NO_3^-	9.9±7.0	8.5±3.9	12.4±10.2	10.2±8.3	7.9±4.2	13.9±11.9	8.1±6.9	6.5±4.1	11.1±10.0
SO_4^{2-}	6.7±3.4	6.2±3.7	7.6±2.7	6.1±2.5	5.1±1.5	7.8±3.1	6.5±2.0	5.6±0.8	8.3±2.3
NH_4^+	4.6±2.7	4.2±1.2	5.3±4.2	5.3±3.2	4.7±1.4	6.4±4.9	3.8±2.5	3.4±1.2	4.6±3.9
Cl^-	0.53±0.40	0.52±0.45	0.56±0.29	0.40±0.16	0.35±0.14	0.48±0.16	0.53±0.41	0.48±0.36	0.61±0.51
Na^+	0.84±0.41	0.85±0.44	0.82±0.35	0.81±0.26	0.82±0.33	0.80±0.14	1.19±0.4	1.21±0.49	1.17±0.12
K+	0.71±0.34	0.6±0.28	0.91±0.35	0.73±0.3	0.57±0.23	0.99±0.2	0.71±0.26	0.57±0.1	0.99±0.24
Mg^{2+}	0.13±0.12	0.11±0.13	0.18±0.09	0.1±0.08	0.05±0.02	0.18±0.07	0.15±0.09	0.09±0.04	0.25±0.08
Ca^{2+}	0.71±0.72	0.58±0.67	0.94±0.77	0.47±0.43	0.22±0.14	0.87±0.45	0.73±0.56	0.4±0.21	1.35±0.49
SNA[b]	21.2±11.2	18.9±5.5	25.4±16.8	21.7±13.4	17.7±5.6	28.2±19.6	18.5±10.7	15.5±5.2	24.0±16.0
WSIIs[c]	24.1±11.5	21.6±6.1	28.8±16.7	24.2±13.5	19.7±5.5	31.5±19.3	21.8±11.1	18.3±5.3	28.4±15.9
NOR	0.20±0.13	0.21±0.11	0.19±0.16	0.18±0.13	0.17±0.08	0.20±0.18	0.15±0.12	0.14±0.10	0.16±0.15
SOR	0.31±0.10	0.33±0.09	0.29±0.11	0.26±0.08	0.26±0.05	0.26±0.12	0.22±0.07	0.23±0.07	0.22±0.08
NO_3^- /SO_4^{2-}	1.61±0.97	1.70±1.04	1.43±0.81	1.67±1.00	1.72±1.11	1.57±0.87	1.20±0.77	1.23±0.80	1.17±0.76

[a] Average value of five sampling sites in WH;
[b] Total concentration of NO_3^-, SO_4^{2-} and NH_4^+;
[c] Total concentration of 8 measured WSIIs.

NO_3^-/SO_4^{2-} ratio is widely used to distinguish mobile sources from stationary sources of nitrogen and sulfur in the atmosphere (Wang et al., 2017; Xu et al., 2019). A high ratio means mobile sources are prominent and vice versa. Over the entire observation, the average NO_3^-/SO_4^{2-} ratio was 1.56, indicating mobile sources such as vehicle exhaust played an important role in $PM_{2.5}$ rather than

stationary sources like coal combustion. Higher NO_3^-/ SO_4^{2-} ratios were observed in the control period compared to the non-control period, indicating the impact of stationary sources control was more prominent than that of mobile sources control. This was in line with the control measures implemented in this campaign which were focused on industries, coal-fired power plants and road dust rather than vehicles.

To explore the secondary transformation of NO_2 to NO_3^- and SO_2 to SO_4^{2-}, nitrogen oxidation ratio (NOR= $nNO_3^-/(nNO_3^-+nNO_2)$) and sulfur oxidation ratio (SOR= $nSO_4^{2-}/(nSO_4^{2-}+nSO_2)$) were calculated (Sun et al., 2006; Zheng et al., 2019). The higher values mean more intensive chemical reactions. In general, SOR (mean 0.29) was higher than NOR (0.19), suggesting stronger secondary transformation of SO_2 to SO_4^{2-} than NO_2 to NO_3^-. The gas-phase oxidation of SO_2 by ·OH to SO_4^{2-} is greatly affected by temperature, while heterogeneous oxidation is positively correlated with relative humidity (Sun et al., 2006). During this observation, NOR was positively correlated (Table S2) with RH (0.51, $p<0.01$) and negatively correlated with T (-0.44, $p<0.01$), while SOR only showed positive correlation with RH (0.38, $p<0.01$), suggesting the major conversion mechanism of SO_2 to SO_4^{2-} and NO_2 to NO_3^- was heterogeneous oxidation.

For NOR, it was higher in the control period than that in non-control period in WH, while it showed the opposite trend in HS and HG. This could be related to the variations in precursors (such as NO_2) and relative humidity. Under the influence of emission source control, NO_2 concentration in the control period is lower than that in the non-control period, leading to a lower NOR in the control period. Higher relative humidity was beneficial to secondary transformation (Tao et al., 2017). It can be found that relative humidity was higher in the control period than that in non-control period, and higher relative humidity was found in WH than HS and HG. SOR showed the same trend (control period > non-control period) at all sampling sites, indicating stronger transformation from SO_2 to SO_4^{2-} in the control period.

Mean concentration of K^+, a tracer of biomass burning, was 0.71 μg m^{-3}, lower than that in Beijing (1.59 μg m^{-3}) and Shijiazhuang (2.55 μg m^{-3}), while it was comparable to that in Beijing during the APEC period (0.73 μg m^{-3}) when open biomass burning activities were well controlled in North China, suggesting the contribution of biomass burning to $PM_{2.5}$ in the study area could be negligible (Zhang

et al., 2017). Additionally, source apportionment of $PM_{2.5}$ in 2014 in WH also manifested the minor contribution of biomass burning to $PM_{2.5}$. Positive correlation (0.45, $p<0.01$) was found between Cl^- and Na^+, indicating the common sources. Cl^-/Na^+ ratio varied from 0.46 to 0.95, lower that from fresh sea salt (1.7), implying sea salt was not the main source of Cl^- and Na^+ (Xu et al., 2019). Given the location of the study area, it is inferred that reduction in Cl^- concentration in the control period was most likely attributed to emission reduction of coal combustion, because Cl^- in $PM_{2.5}$ can be emitted from coal combustion process (Xu et al., 2019). However, no significant difference in Na^+ concentration was observed, indicating the complexity of its source. Ca^{2+} and Mg^{2+}, as tracers for terrestrial sources, are mainly originated from road dust and construction sites (Xu et al., 2019). High correlation (0.82, $p<0.01$) between them indicated their similar origins. Compared with the non-control period, the concentration of Ca^{2+} and Mg^{2+} were 48.5% and 47.4% lower in the control period, which was consistent with the control measures of road dust and construction works in control period.

3.3.2 OC and EC

Carbonaceous species including OC and EC were another dominant component of $PM_{2.5}$ (Table 4). The mean concentrations (μg m^{-3}) of OC (EC) were 7.7 (3.0), 9.7 (3.5) and 8.3 (3.4) for WH, HG and HS during the sampling campaign, accounting for an average of 12% (4.6%), 14.1% (4.9%) and 11.3% (4.5%) of $PM_{2.5}$ mass concentration, respectively. In comparison with other short-term control events in China, levels of OC and EC during this study were lower than those observed in the Asian Games and APEC, but a little higher than those in the Victory Day Parade and the G20 (Table S3).

Table 4 Mean values of OC, EC, SOC, OC/EC ratio and SOC percentage of OC during control and non-control period

Species (μg m^{-3})	WH			HG			HS		
	Mean	Control	Non-control	Mean	Control	Non-control	Mean	Control	Non-control
OC	7.7±2.9	6.4±2.3	10.0±2.6	9.7±3.8	7.9±2.9	12.7±3.3	8.3±3.4	6.6±1.6	11.4±3.7
EC	3.0±1.4	2.5±1.2	4.1±1.3	3.5±1.7	2.7±1.0	4.9±1.7	3.4±1.2	2.6±0.4	4.8±1.1
SOC	4.3±2.1	3.6±1.7	5.4±2.2	5.8±2.5	4.9±2.2	7.2±2.5	4.4±2.4	3.6±1.4	6.0±3.3
OC/EC	2.7±0.68	2.76±0.67	2.58±0.69	2.98±0.82	3.09±0.80	2.79±0.88	2.47±0.57	2.51±0.53	2.40±0.67
SOC/OC (%)	54.9±14.0	55.9±13.9	52.9±14.2	59.3±10.4	61.0±9.5	56.4±11.8	51.8±11.6	53.2±9.7	49.3±15.0

Similar to SNA, significant reductions of OC and EC were observed during control period - of 36% and 39%, 37.8% and 44.9%, 42.1% and 45.8% for WH, HG and HS, respectively, compared with those in non-control period. This was consistent with other studies in some mega-events, when lower OC and EC concentrations were observed during the control period (Chen et al., 2021; Xu et al., 2019). EC is mainly derived from combustion processes, while OC can be formed by photochemical reactions (secondary OC, SOC) except for direct emission (Cao et al., 2007; Ji et al., 2019). A significant positive correlation (0.76, $p<0.01$) was found between OC and EC (Table S2), indicating their similar sources - such as vehicle emission and coal combustion. OC/EC ratio was widely used to distinguish their sources, and an OC/EC ratio >2 usually indicated the presence of SOC (Cao et al., 2007). Additionally, higher OC/EC ratios were found from biomass burning (4.1-14.5) and coal combustion (0.3-12) than that from vehicle emission (1.1-5.0) (Cao et al., 2007; Ji et al., 2019; Watson et al., 2001; Zheng et al., 2006). Average OC/EC ratios ranged from 2.47 to 2.99 over the entire sampling period, indicating the mixed sources and the presence of SOC. A higher OC/EC ratio was observed in the control period, which was contrary to some studies. In this study, private cars were allowed on the road during the control period, while there was a limitation for trucks. A higher OC/EC ratio was found from gasoline vehicles (4.13) than from diesel vehicles (2.03) in WH (Huang et al., 2022). In addition, HG (2.98) had a higher OC/EC ratio than that in WH (2.7) and HS (2.47) over the entire observation period, which can be explained by more biomass burning in HG due to its larger proportion of agricultural activities.

SOC was estimated by the method based on OC/EC ratio proposed by Castro et al. (1999), which was defined as $SOC=OC-EC\times(OC/EC)_{min}$, where $(OC/EC)_{min}$ means the minimum OC/EC ratio. OC/EC ratio and SOC/OC are shown in Table 4. The estimated SOC concentration was in a range of 3.9-5.8 μg m^{-3}, accounting for 50.2%-59.3% of OC, indicating the large contribution of SOC to OC in $PM_{2.5}$ during this study period. Higher temperature was favorable for SOC formation (Xu et al., 2019). In this study, SOC was significantly positively correlated with temperature (0.59, $p<0.01$). Lower SOC concentration (3.8±1.8 μg m^{-3}) was found in the control period with lower temperature (18.4±3.0 °C) than that in non-control period (5.8±2.5 μg m^{-3}, 19.6±1.5 °C). Though the concentration

of SOC was lower in the control period, it contributed a larger proportion compared with the non-control period, indicating the important role of SOC when the primary emissions were well controlled. It can be inferred that with the further reduction of SO_2 and NO_x in China, SOC would play a relatively more important role in air pollution.

3.3.3 Trace elements

As shown in Table 5, the total concentration of 10 measured trace elements ($\sum_{10}$TEs) was lower in the control period (236.6-700.8 ng m^{-3}) than in the non-control period (363.4-929.9 ng m^{-3}). Cu and Zn were the most abundant species, with average values of 104.6±191.4 ng m^{-3} and 102.3±59.9 ng m^{-3}, respectively. There was positive correlation between Cu and Zn (0.31, $p<0.01$, Table S4), indicating their similar sources. Cu and Zn are derived from a variety of sources, such as vehicle emission, brake wear, coal combustion and metal smelting (Pant and Harrison, 2013; Thorpe and Harrison, 2008). Lower concentrations of Cu, Zn, Pb and Cd were observed in the control period, with reductions of 24.8%, 30.7%, 29.1% and 22.2%, respectively. Unleaded gasoline has been used in China since 1997, so Pb is often thought to be from coal combustion (Tian et al., 2015). Cd is usually identified to be from coal combustion (Liu et al., 2018a). These trends showed the reduction of coal combustion emission, which was consistent with the controls on coal-fired power plants and industries. However, As, a typical marker of coal combustion (Tian et al., 2015), had no obvious change in concentration, which could be related to the air masses during the control period being from Shandong, Hebei and Henan, provinces with large coal consumption (see Fig.S3).

Table 5 Mass concentration of measured trace elements during the control and non-control periods

Species	WH			HG			HS		
(ng m^{-3})	Mean	Control	Non-control	Mean	Control	Non-control	Mean	Control	Non-control
V	2.1±1.1	1.7±0.9	2.9±1.0	3.6±1.7	2.5±0.6	5.4±1.5	3.7±1.8	2.8±0.9	5.5±1.5
Cr	20.6±10.3	20.4±12.2	20.8±5.9	26.9±6.0	25.5±6.9	29.2±3.1	32.9±8.0	30.5±6.8	37.6±8.3
Mn	40.3±27.1	25.6±18.2	65.3±20.6	58.8±32.4	39.9±21.0	89.5±22.6	55.1±29.2	38.6±16.7	86.1±20.9
Co	0.7±0.3	0.6±0.1	0.9±0.4	1.0±0.4	0.8±0.3	1.5±0.3	1.0±0.3	0.8±0.2	1.3±0.3
Ni	25.6±9.2	25.3±8.2	26.1±10.8	35.4±14.3	33.8±15.8	37.9±12.1	41.0±9.9	42.0±12.3	39.3±1.7
Cu	53.6±164.8	43.7±173.8	70.5±148.9	105.2±116.3	116.9±124.6	86.2±106.5	343.6±186.1	297.8±142.3	429.5±235.4
Zn	85.9±43.5	69.8±34.8	113.3±43.5	121.2±51.1	107.6±44.9	143.4±55.7	162.1±87.2	153.5±101.3	178.3±54.2
As	30.4±7.7	29.7±7.5	31.4±8.0	39.7±3.6	38.6±3.2	41.4±3.8	49.7±13.9	50.7±15.8	47.9±10.1
Cd	0.6±0.3	0.5±0.2	0.8±0.3	0.8±0.6	0.9±0.8	0.8±0.2	1.4±1.4	1.4±1.6	1.4±0.9

Pb	23.8±9.6	19.4±6.1	31.3±9.8	26.6±9.4	22.1±7.1	33.9±8.2	89.8±101.9	82.8±106.0	103.0±99.2
$\sum_{10}$TEs[a]	283.6±179.3	236.6±175.8	363.4±157.3	419.3±177.5	388.6±188.5	469.1±156.4	780.5±287.3	700.8±247.6	929.9±312.5

[a] Total concentration of 10 measured trace elements.

Significant reduction of Co (30%) was observed in the control period, which could be attributed to the control on road dust, construction sites and frequent roads cleaning (de la Campa et al., 2010). V is related to heavy oil combustion, especially for ship emissions (Pandolfi et al., 2011; Salameh et al., 2015). WH, located in the middle reaches of the Yangtze River, is an important port and shipping center in China. In Oct 2019, canalage goods volume in Hubei Province was 42.63 million tons, a little lower than that in Shanghai (58.4 million tons), a famous port city in China. Therefore, the reduction of V can be attributed to the decreased ship emission during control period. Ni is often associated with fuel combustion (Lin et al., 2020). In this study, the ratio of V/Ni was 0.1 on average, lower than 2.3-3.5 which was characterized for ship emissions (Pandolfi et al., 2011; Salameh et al., 2015), indicating other sources for Ni.

Less reduction of Cr (7%), a tracer of vehicle emission (Lin et al., 2020), than Cd, Pb, Zn and Co was observed, which was consistent with the lax control on traffic. Different from Cr, Mn is usually related to vehicle emission (Wahlin et al., 2006), had a larger reduction (59%), indicating there might be other sources for Mn besides vehicle emission, such as road dusts, metal smelting and electrode material production (Crilley et al., 2017).

3.4 Implications

To ensure air quality during the 7th MWG, atmospheric environment quality management measures were implemented, mainly concentrated on coal-fired power plants and industries, ship emission, construction sites and road dust. As expected, concentrations of $PM_{2.5}$ and its major chemical components (SNA, OC, EC and TEs) were significantly lower in the control period than in the non-control period. However, higher contributions of secondary components such as SNA and SOC to $PM_{2.5}$ were observed, due to the favorable meteorological conditions for secondary transformation. No significant increase of O_3 concentration was observed during the control period, different from other short-term control events which pointed out that elevated O_3 concentrations were attributed to less NO_x

emissions from vehicles. In this study, no strict control measures were taken for vehicles, indicating $PM_{2.5}$ and O_3 need to be coordinated control. In the future of air pollution control, the non-linear relationship between $PM_{2.5}$ and O_3 should be taken into consideration. Additionally, similar temporal variation of $PM_{2.5}$ and its chemical components were found at different sampling sites, and some elevated chemical components (such as As) were linked to air masses from the north during the control period, indicating the importance of regional joint prevention and control.

4 Conclusions

Good air quality was observed during the 7th MWG, helped by a series of temporary control measures. We evaluated the effect of control measures based on $PM_{2.5}$ chemical composition. Mass concentration of $PM_{2.5}$ was 50.2-60.4 μg m^{-3} during the control period in study areas, which was 29.6-44.8% lower than in the non-control period. The dominant chemical species, including WSIIs, OC, EC and TEs were lower by 22.8-37.5%, 18.1-43.5%, 23.5-45.8% and 17.2-39.2%, respectively, in the control period. However, a higher contribution of secondary species (SNA and SOC) were observed during the control period due to the favorable meteorological conditions for secondary transformation. This indicated the important role of secondary transformation under relatively low $PM_{2.5}$ concentration. By comparing air masses from the same region, lower $PM_{2.5}$ concentrations were found in the control period than the non-control period. Additionally, concentrations of coal combustion related trace elements (e.g. Cu, Zn, Cd, Pb) and road dust related trace elements (e.g. Co) were lower in the control period. These all indicated the reduction of anthropogenic emissions during the control period. However, minor variation of As was found in this study due to the influence of northern air mass. To effectively improve air quality in the future, attention should be paid to the reduction of primary particulate matter as well as precursors of secondary components. In addition to the reduction of local emissions, the impact of regional transport should also be considered.

Acknowledgments

We sincerely thank Yewang Su, An Xu, Xingyu Li, Jinxu Hu, Yue Jiao, Yangshuo Liang, Wen Pi, Hanfei Wang, Xinyu Zhao and Jiaoping Li for sample collection. This work was funded by the

National Key Research and Development Program of China (No. 2017YFC0212603). Yao Mao acknowledges financial supports from the China Scholarship Council (No.202006410024).

References

Ansari, T.U., Wild, O., Li, J., Yang, T., Xu, W., Sun, Y., Wang, Z., 2019. Effectiveness of short-term air quality emission controls: a high-resolution model study of Beijing during the Asia-Pacific Economic Cooperation (APEC) summit period. Atmos. Chem. Phys. 19, 8651-8668.

Cao, J.J., Lee, S.C., Chow, J.C., Watson, J.G., Ho, K.F., Zhang, R.J., Jin, Z.D., Shen, Z.X., Chen, G.C., Kang, Y.M., Zou, S.C., Zhang, L.Z., Qi, S.H., Dai, M.H., Cheng, Y., Hu, K., 2007. Spatial and seasonal distributions of carbonaceous aerosols over China. J. Geophys. Res. 112, D22S11.

Castro, L.M., Pio, C.A., Harrison, R.M., Smith, D.J.T., 1999. Carbonaceous aerosol in urban and rural European atmospheres: estimation of secondary organic carbon concentrations. Atmos. Environ. 33, 2771-2781.

Chen, K., Metcalfe, S.E., Yu, H., Xu, J., Xu, H., Ji, D., Wang, C., Xiao, H., He, J., 2021. Characteristics and source attribution of $PM_{2.5}$ during 2016 G20 Summit in Hangzhou: Efficacy of radical measures to reduce source emissions. J. Environ. Sci. 106, 47-65.

Chow, J.C., Watson, J.G., Chen, L.W., Chang, M.C., Robinson, N.F., Trimble, D., Kohl, S., 2007. The IMPROVE_A temperature protocol for thermal/optical carbon analysis: maintaining consistency with a long-term database. J. Air Waste Manage. Assoc. 57, 1014-1023.

Crilley, L.R., Lucarelli, F., Bloss, W.J., Harrison, R.M., Beddows, D.C., Calzolai, G., Nava, S., Valli, G., Bernardoni, V., Vecchi, R., 2017. Source apportionment of fine and coarse particles at a roadside and urban background site in London during the 2012 summer ClearfLo campaign. Environ. Pollut. 220, 766-778.

de la Campa, A.M.S., de la Rosa, J.D., Gonzalez-Castanedo, Y., Fernandez-Camacho, R., Alastuey, A., Querol, X., Pio, C., 2010. High concentrations of heavy metals in PM from ceramic factories of Southern Spain. Atmos. Res. 96, 633-644.

Gao, M., Liu, Z., Wang, Y., Lu, X., Ji, D., Wang, L., Li, M., Wang, Z., Zhang, Q., Carmichael, G.R., 2017. Distinguishing the roles of meteorology, emission control measures, regional transport, and co-benefits of reduced aerosol feedbacks in "APEC Blue". Atmos. Environ. 167, 476-486.

Guo, S., Hu, M., Zamora, M.L., Peng, J., Shang, D., Zheng, J., Du, Z., Wu, Z., Shao, M., Zeng, L., Molina, M.J., Zhang, R., 2014. Elucidating severe urban haze formation in China. PNAS 111, 17373-17378.

Huang, F., Zhou, J., Chen, N., Li, Y., Li, K., Wu, S., 2019. Chemical characteristics and source apportionment of $PM_{2.5}$ in Wuhan, China. J. Atmos. Chem. 76, 245-262.

Huang, H., Zhang, J., Hu, H., Kong, S., Qi, S., Liu, X., 2022. On-road emissions of fine particles and associated chemical components from motor vehicles in Wuhan, China. Environ. Res. 210, 112900.

Huang, K., Zhuang, G., Lin, Y., Wang, Q., Fu, J.S., Fu, Q., Liu, T., Deng, C., 2013. How to improve the air quality over megacities in China: pollution characterization and source analysis in Shanghai before, during, and after the 2010 World Expo. Atmos. Chem. Phys. 13, 5927-5942.

Hyslop, N.P., 2009. Impaired visibility: the air pollution people see. Atmos. Environ. 43, 182-195.

Ji, D., Gao, M., Maenhaut, W., He, J., Wu, C., Cheng, L., Gao, W., Sun, Y., Sun, J., Xin, J., Wang, L., Wang, Y., 2019. The carbonaceous aerosol levels still remain a challenge in the Beijing-Tianjin-Hebei region of China: Insights from continuous high temporal resolution measurements in multiple cities. Environ. Int. 126, 171-183.

Kim, K.H., Kabir, E., Kabir, S., 2015. A review on the human health impact of airborne particulate matter. Environ. Int. 74, 136-143.

Li, H., Wang, D., Cui, L., Gao, Y., Huo, J., Wang, X., Zhang, Z., Tan, Y., Huang, Y., Cao, J., Chow, J.C., Lee, S.C., Fu, Q., 2019a. Characteristics of atmospheric $PM_{2.5}$ composition during the implementation of stringent pollution control measures in shanghai for the 2016 G20 summit. Sci. Total Environ. 648, 1121-1129.

Li, K., Jacob, D.J., Liao, H., Zhu, J., Shah, V., Shen, L., Bates, K.H., Zhang, Q., Zhai, S., 2019b. A two-pollutant strategy for improving ozone and particulate air quality in China. Nat. Geosci. 12, 906-910.

Li, R., Mei, X., Chen, L., Wang, L., Wang, Z., Jing, Y., 2020a. Long-term (2005–2017) view of atmospheric pollutants in Central China using multiple satellite observations. Remote Sens. 12, 1041.

Li, W., Shao, L., Wang, W., Li, H., Wang, X., Li, Y., Li, W., Jones, T., Zhang, D., 2020b. Air quality improvement in response to intensified control strategies in Beijing during 2013-2019. Sci. Total Environ. 744, 140776.

Lin, Y.C., Zhang, Y.L., Song, W.H., Yang, X.Y., Fan, M.Y., 2020. Speci fic sources of health risks caused by size -resolved PM -bound metals in a typical coal -burning city of northern China during the winter haze event. Sci. Total Environ. 734, 138651.

Liu, J.W., Chen, Y.J., Chao, S.H., Cao, H.B., Zhang, A.C., Yang, Y., 2018a. Emission control priority of $PM_{2.5}$-bound heavy metals in different seasons: A comprehensive analysis from health risk perspective. Sci. Total Environ. 644, 20-30.

Liu, S., Hua, S., Wang, K., Qiu, P., Liu, H., Wu, B., Shao, P., Liu, X., Wu, Y., Xue, Y., Hao, Y., Tian, H., 2018b. Spatial-temporal variation characteristics of air pollution in Henan of China: Localized emission inventory, WRF/Chem simulations and potential source contribution analysis. Sci. Total Environ. 624, 396-406.

Ma, T., Duan, F., He, K., Qin, Y., Tong, D., Geng, G., Liu, X., Li, H., Yang, S., Ye, S., Xu, B., Zhang, Q., Ma, Y., 2019. Air pollution characteristics and their relationship with emissions and meteorology in the Yangtze River Delta region during 2014-2016. J. Environ. Sci. 83, 8-20.

Mi, K., Zhuang, R., Zhang, Z., Gao, J., Pei, Q., 2019. Spatiotemporal characteristics of $PM_{2.5}$ and its associated gas pollutants, a case in China. Sustain. Cities Soc. 45, 287-295.

Pandolfi, M., Gonzalez-Castanedo, Y., Alastuey, A., de la Rosa, J.D., Mantilla, E., de la Campa, A.S., Querol, X., Pey, J., Amato, F., Moreno, T., 2011. Source apportionment of PM_{10} and $PM_{2.5}$ at multiple sites in the strait of Gibraltar by PMF: impact of shipping emissions. Environ. Sci. Pollut. Res. 18, 260-269.

Pant, P., Harrison, R.M., 2013. Estimation of the contribution of road traffic emissions to particulate matter concentrations from field measurements: A review. Atmos. Environ. 77, 78-97.

Pui, D.Y.H., Chen, S.-C., Zuo, Z., 2014. $PM_{2.5}$ in China: Measurements, sources, visibility and health effects, and mitigation. Particuol. 13, 1-26.

Salameh, D., Detournay, A., Pey, J., Perez, N., Liguori, F., Saraga, D., Bove, M.C., Brotto, P., Cassola, F., Massabo, D., Latella, A., Pillon, S., Formenton, G., Patti, S., Armengaud, A., Piga, D., Jaffrezo, J.L., Bartzis, J., Tolis, E., Prati, P., Querol, X., Wortham, H., Marchand, N., 2015. $PM_{2.5}$ chemical composition in five European Mediterranean cities: A 1-year study. Atmos. Res. 155, 102-117.

Schleicher, N., Norra, S., Chen, Y., Chai, F., Wang, S., 2012. Efficiency of mitigation measures to reduce particulate air pollution-a case study during the Olympic Summer Games 2008 in Beijing, China. Sci. Total Environ. 427-428, 146-158.

Su, F., Xu, Q., Wang, K., Yin, S., Wang, S., Zhang, R., Tang, X., Ying, Q., 2021. On the effectiveness of short-term intensive emission controls on ozone and particulate matter in a heavily polluted megacity in central China. Atmos. Environ. 246, 118111.

Sun, Y., Zhuang, G., Tang, A., Wang, Y., An, Z., 2006. Chemical characteristics of $PM_{2.5}$ and PM_{10} in haze−fog episodes in Beijing. Environ. Sci. Technol. 40, 3148-3155.

Tao, J., Zhang, L., Cao, J., Zhang, R., 2017. A review of current knowledge concerning $PM_{2.5}$ chemical composition, aerosol optical properties and their relationships across China. Atmos. Chem. Phys. 17, 9485-9518.

Tao, J., Zhang, L., Zhang, Z., Huang, R., Wu, Y., Zhang, R., Cao, J., Zhang, Y., 2015. Control of $PM_{2.5}$ in Guangzhou during the 16th Asian Games period: implication for hazy weather prevention. Sci. Total Environ. 508, 57-66.

Thorpe, A., Harrison, R.M., 2008. Sources and properties of non-exhaust particulate matter from road traffic: A review. Sci. Total Environ. 400, 270-282.

Tian, H.Z., Zhu, C.Y., Gao, J.J., Cheng, K., Hao, J.M., Wang, K., Hua, S.B., Wang, Y., Zhou, J.R., 2015. Quantitative assessment of atmospheric emissions of toxic heavy metals from anthropogenic sources in China: historical trend, spatial distribution, uncertainties, and control policies. Atmos. Chem. Phys. 15, 10127-10147.

Wahlin, P., Berkowicz, R., Palmgren, F., 2006. Characterisation of traffic-generated particulate matter in Copenhagen. Atmos. Environ. 40, 2151-2159.

Wang, S., Yan, Y., Yu, R., Shen, H., Hu, G., Wang, S., 2021. Influence of pollution reduction interventions on atmospheric $PM_{2.5}$: A case study from the 2017 Xiamen. Atmos. Pollut. Res. 12, 101137.

Wang, Y., Xue, Y., Tian, H., Gao, J., Chen, Y., Zhu, C., Liu, H., Wang, K., Hua, S., Liu, S., Shao, P., 2017. Effectiveness of temporary control measures for lowering $PM_{2.5}$ pollution in Beijing and the implications. Atmos. Environ. 157, 75-83.

Watson, J.G., Chow, J.C., Houck, J.E., 2001. $PM_{2.5}$ chemical source profiles for vehicle exhaust, vegetative burning, geological material, and coal burning in Northwestern Colorado during 1995. Chemosphere 43, 1141-1151.

Wu, X., Shi, G., Xiang, X., Yang, F., 2021. The characteristics of $PM_{2.5}$ pollution episodes during 2016–2019 in Sichuan Basin, China. Aerosol Air Qual. Res. 21, 210126.

Xu, W., Liu, X., Liu, L., Dore, A.J., Tang, A., Lu, L., Wu, Q., Zhang, Y., Hao, T., Pan, Y., Chen, J., Zhang, F., 2019. Impact of emission controls on air quality in Beijing during APEC 2014: Implications from water-soluble ions and carbonaceous aerosol in $PM_{2.5}$ and their precursors. Atmos. Environ. 210, 241-252.

Yan, F., Chen, W., Jia, S., Zhong, B., Yang, L., Mao, J., Chang, M., Shao, M., Yuan, B., Situ, S., Wang, X., Chen, D., Wang, X., 2020. Stabilization for the secondary species contribution to $PM_{2.5}$ in the Pearl River Delta (PRD) over the past decade, China: A meta-analysis. Atmos. Environ. 242, 117817.

Yang, X., Zhang, T., Zhang, Y., Chen, H., Sang, S., 2021. Global burden of COPD attributable to ambient $PM_{2.5}$ in 204 countries and territories, 1990 to 2019: A systematic analysis for the Global Burden of Disease Study 2019. Sci. Total Environ. 796, 148819.

Zhang, Q., Zheng, Y., Tong, D., Shao, M., Wang, S., Zhang, Y., Xu, X., Wang, J., He, H., Liu, W., Ding, Y., Lei, Y., Li, J., Wang, Z., Zhang, X., Wang, Y., Cheng, J., Liu, Y., Shi, Q., Yan, L., Geng, G., Hong, C., Li, M., Liu, F., Zheng, B., Cao, J., Ding, A., Gao, J., Fu, Q., Huo, J., Liu, B., Liu, Z., Yang, F., He, K., Hao, J., 2019. Drivers of improved $PM_{2.5}$ air quality in China from 2013 to 2017. PNAS 116, 24463-24469.

Zhang, Y., Hong, Z., Chen, J., Xu, L., Hong, Y., Li, M., Hao, H., Chen, Y., Qiu, Y., Wu, X., Li, J.-R., Tong, L., Xiao, H., 2020. Impact of control measures and typhoon weather on characteristics and formation of $PM_{2.5}$ during the 2016 G20 summit in China. Atmos. Environ. 224, 117312.

Zhang, Y., Kang, S., 2018. Characteristics of carbonaceous aerosols analyzed using a multiwavelength thermal/optical carbon analyzer: A case study in Lanzhou City. Sci. China Earth Sci. 62, 389-402.

Zhang, Z., Gao, J., Zhang, L., Wang, H., Tao, J., Qiu, X., Chai, F., Li, Y., Wang, S., 2017. Observations of biomass burning tracers in $PM_{2.5}$ at two megacities in North China during 2014 APEC summit. Atmos. Environ. 169, 54-64.

Zheng, H., Kong, S., Chen, N., Yan, Y., Liu, D., Zhu, B., Xu, K., Cao, W., Ding, Q., Lan, B., Zhang, Z., Zheng, M., Fan, Z., Cheng, Y., Zheng, S., Yao, L., Bai, Y., Zhao, T., Qi, S., 2020. Significant changes in the chemical compositions and sources of $PM_{2.5}$ in Wuhan since the city lockdown as COVID-19. Sci. Total Environ. 739, 140000.

Zheng, H., Kong, S., Yan, Q., Wu, F., Cheng, Y., Zheng, S., Wu, J., Yang, G., Zheng, M., Tang, L., Yin, Y., Chen, K., Zhao, T., Liu, D., Li, S., Qi, S., Zhao, D., Zhang, T., Ruan, J., Huang, M., 2019. The impacts of pollution control measures on $PM_{2.5}$ reduction: Insights of chemical composition, source variation and health risk. Atmos. Environ. 197, 103-117.

Zheng, M., Hagler, G.S.W., Ke, L., Bergin, M.H., Wang, F., Louie, P.K.K., Salmon, L., Sin, D.W.M., Yu, J.Z., Schauer, J.J., 2006. Composition and sources of carbonaceous aerosols at three contrasting sites in Hong Kong. J. Geophys. Res. 111, D20313.